

Decay of a plasmon into neutral modes in a carbon nanotube

Wei Chen and A. V. Andreev

Department of Physics, University of Washington, Seattle, WA 98195-1560, USA

E. G. Mishchenko

Department of Physics and Astronomy, University of Utah, Salt Lake City, Utah 84112, USA

L. I. Glazman

Department of Physics, Yale University, New Haven, CT 06520, USA

We evaluate the rate of energy loss of a plasmon in a disorder-free carbon nanotube. The plasmon decays into neutral bosonic excitations of the electron liquid. The process is mediated either by phonon-assisted backscattering of a single electron or Umklapp backscattering of two electrons. To lowest order in the backscattering interactions the partial decay rates are additive. At zero doping the corresponding decay rates scale as power-laws of the temperature with positive and negative exponents for the two mechanisms, respectively. The precise values of the exponents depend on the Luttinger liquid parameter. At finite doping the decay rates are described by universal crossover functions of frequency and chemical potential measured in units of temperature. In the evaluation of the plasmon decay, we concentrate on a finite-length geometry allowing excitation of plasma resonances.

I. INTRODUCTION

Electronic properties of single wall carbon nanotubes (CNTs) have been studied intensively in the DC limit by means of electron transport¹, by optical excitations²⁻⁶, and by angle-resolved electron energy loss spectroscopy in the UV region⁷. CNT properties in the intermediate (THz) band of frequencies are harder to access experimentally and consequently they attracted less attention in theory. The dominant excitations in that frequency range are plasmons. Initial experiments probing them by means of time-resolved measurements were reported recently⁸. Here we are interested in the intrinsic mechanisms of the decay of plasmons into other excitations within a metallic (armchair) CNT.

The existing tunneling experiments provide support for the Luttinger liquid description of the charge carriers in CNTs^{9,10}. In that description, the collective excitation, plasmon, is just one of the eigenmodes with linear spectrum. As such, it does not decay.

In the conventional Fermi liquid description applicable to higher-dimensional conductors, separation of excitations into plasmons and Fermi-quasiparticles is not exact, leading to a plasmon decay by exciting quasiparticles¹¹. In contrast, in one-dimensional conductors quasiparticles are ill-defined, and plasmon decays into other collective excitations of the electron liquid.

In armchair nanotubes in addition to the plasmon mode the spectrum of bosonic low energy excitations of electron liquid contains three neutral modes propagating with the Fermi velocity. Conservation of energy and momentum allows a plasmon decay into neutral modes, as illustrated in Fig. 1. However absence of coupling between the bosonic modes in the Luttinger liquid description precludes the possibility of plasmon decay. It arises from backscattering interactions and thus requires

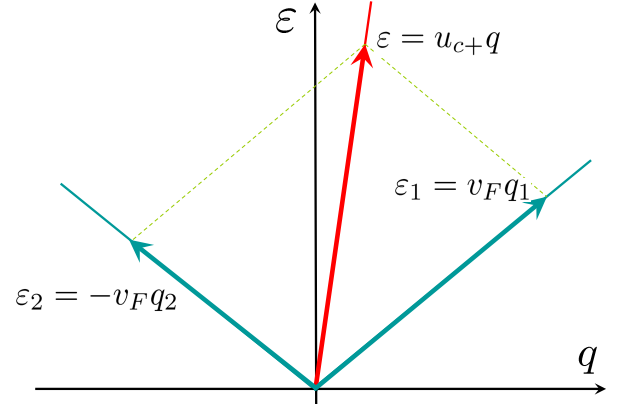


FIG. 1: (Color online) Schematic picture of a possible decay process of a plasmon excitation with momentum q and energy $\epsilon = u_{c+}q$ into two neutral mode excitations with momenta q_1 and q_2 and energies $\epsilon_1 = v_F q_1$ and $\epsilon_2 = -v_F q_2$. The line with the steep slope represents the plasmon mode with velocity u_{c+} and the two lines with shallower slopes represent neutral modes with velocities $\pm v_F$. Conservation of energy and momentum requires $\epsilon = \epsilon_1 + \epsilon_2$ and $q = q_1 + q_2$.

consideration of corrections to the Luttinger liquid approximation.

Another qualitative difference between plasmon decay in nanotubes from that in higher dimensions is that in one dimension the excitations of neutral modes generated during the plasmon decay can propagate only in two distinct directions. The plasmon decay products propagating along the same direction may recombine into a plasmon. Therefore in long devices perturbative treatment of plasmon decay, strictly speaking, is not justified.

In this paper we consider plasmon decay in a finite geometry illustrated in Fig. 2. In this experimentally motivated¹² setup a carbon nanotube connected to two

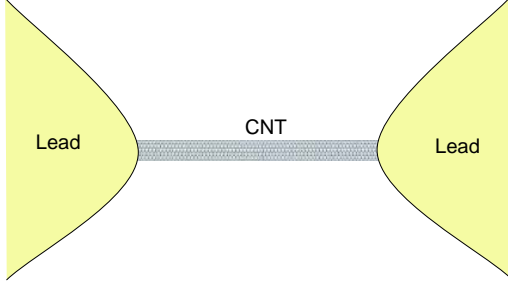


FIG. 2: (Color online) Schematic representation of the device. A carbon nanotube (CNT) connected to two metal leads is subjected to ac-electric field.

metal leads is subjected to THz electric field. The finite length of the device enables us to account for the plasmon decay processes using perturbation theory in the backscattering interactions. We investigate how the decay processes affect the plasmon resonances and modify the device conductance.

The paper is organized as follows. In Sec. II we present the Luttinger liquid description of electron liquid in armchair carbon nanotubes. In Sec. III we obtain the ac conductance of the device in the absence of plasmon decay into the neutral modes. In Sec. IV we discuss the physical mechanisms of plasmon decay and study their influence on energy dissipation in the ac conductance of the device. Our results are summarized in Sec. V.

II. LUTTINGER LIQUID DESCRIPTION OF ARMCHAIR CNTS

Near the Fermi level the electron band structure in armchair nanotubes consists of two spin degenerate bands crossing at two points, $k = \pm Q$, in the Brillouin zone. Near the crossing points the spectrum has linear Dirac-like dispersion, see Fig. 3. For undoped tubes the the Fermi level goes through the crossing points. Setting $\hbar = 1$ we write the non-interacting electron Hamiltonian near the Fermi level as

$$H_0 = -iv_F \sum_{\alpha r \sigma} \int dx \psi_{\alpha r \sigma}^\dagger(x) r \partial_x \psi_{\alpha r \sigma}(x). \quad (1)$$

Here $v_F \approx 8 \times 10^5 \text{ ms}^{-1}$ is the Fermi velocity, $\alpha = \pm 1$ is the valley index, $r = \pm 1$ represents right- and left- moving electrons, and σ is the electron spin. The electron creation/annihilation operators are denoted by ψ^\dagger/ψ . It is important to note that armchair CNT are symmetric about a plane containing the tube axis and bisecting the AB bonds that point along the circumference. As

a result the electron wave functions can be classified by parity $P = -\alpha r = \pm 1$, as indicated in Fig. 3. The wave functions with positive/negative parity are respectively even/odd in the AB sublattices.

We consider an (N, N) armchair CNT, which has N unit cells around the circumference of the tube, and use $1/N$ as a small parameter in the theory. For most synthetic CNTs $N \geq 8$, and this is a good approximation.

For $1/N \ll 1$ the forward scattering part of the e-e interaction is much stronger than the backscattering part, the latter being small by $1/N^{13}$. The former can be written as

$$H_p = \frac{g_p}{2} \int dx n^2(x), \quad n(x) = \sum_{\alpha r \sigma} \psi_{\alpha r \sigma}^\dagger(x) \psi_{\alpha r \sigma}(x). \quad (2)$$

We assume that the Coulomb interaction is screened, e.g. by a gate at a distance d , which is assumed to be short compared to the length of the tube, L but longer than the CNT radius R . The latter can be expressed in terms of the graphene lattice constant a as $R = \sqrt{3}Na/2\pi$. Elementary electrostatics leads to the estimate $g_p \approx 2e^2 \ln(d/R)$.

Thus to zeroth order in $1/N$ backscattering is absent, and electrons in an armchair tube form a Luttinger liquid^{14,15}. The Hamiltonian is bosonized by the standard procedure (see, for example, Refs. 17,18)

$$\psi_{\alpha r \sigma}(x) = \frac{F_{\alpha \sigma}}{\sqrt{2\pi\xi}} \exp\{i[\Theta_{\alpha \sigma}(x) - r \Phi_{\alpha \sigma}(x) + rk_F x]\}. \quad (3)$$

Here $F_{\alpha \sigma}$ are the Klein factors, ξ is a short distance cut-off on the order of the radius of the nanotube, k_F is the Fermi wavevector counted from the Dirac point and Φ and Θ are bosonic fields satisfying the commutation relation $[\Phi_{\alpha \sigma}(x), \Theta_{\alpha' \sigma'}(x')] = -i\delta_{\alpha \alpha'}\delta_{\sigma \sigma'}\theta(x - x')$, where $\theta(x - x')$ is the step function.

Introducing the symmetric and antisymmetric combinations of charge and spin modes in the different valleys,

$$\begin{aligned} \Phi_{\alpha \sigma} &= [\Phi_{c+} + \alpha \Phi_{c-} + \sigma \Phi_{s+} + \alpha \sigma \Phi_{s-}] / 2, \\ \Theta_{\alpha \sigma} &= [\Theta_{c+} + \alpha \Theta_{c-} + \sigma \Theta_{s+} + \alpha \sigma \Theta_{s-}] / 2, \end{aligned} \quad (4)$$

we rewrite the Luttinger liquid Hamiltonian of the CNT including forward scattering as

$$H_0 + H_p = \sum_j \frac{u_j}{2\pi} \int dx [K_j^{-1} (\partial_x \Phi_j)^2 + K_j (\partial_x \Theta_j)^2]. \quad (5)$$

Here $j = c\pm, s\pm$, and the velocity and Luttinger parameter of the j -th mode are related via $u_j = v_F/K_j$. All four bosonic modes have linear spectrum, $\varepsilon_j = u_j|k|$. For the three neutral modes $j = c-, s\pm$, the Luttinger parameter K_j is equal to unity and their velocities coincide with the Fermi velocity. For the charge mode, $j = c+$, the Luttinger parameter is significantly smaller than one, $K_{c+} = 1/\sqrt{1 + 4g_p/\pi v_F} \approx 0.2$. For the reason, the plasmon mode has a much higher velocity than that for the three neutral modes. Below we denote the plasmon velocity by $u \equiv v_F/K_{c+}$.

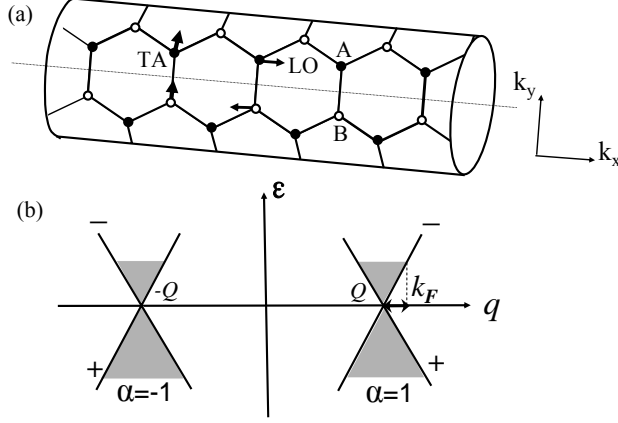


FIG. 3: (a) Schematic picture of an armchair tube. Full and open circles denote atoms in the A and B sublattices. The arrows show atomic displacements in the TA and LO phonon modes. (b) Free electron spectrum of armchair carbon nanotubes: + and - denote the parity of the bands. The two valleys are labeled by the index $\alpha = \pm 1$.

In the absence of decay processes the energy of a plasmon excited in the device dissipates only due to its emission into the leads. The power dissipation due to this mechanism is considered in the next section.

III. PLASMON RESONANCE IN THE ABSENCE OF INTRINSIC DISSIPATION

We consider the setup shown in Fig. 2. The plasmons excited in the tube get partially reflected from the junctions with the leads. The plasmon reflection processes can be described by a one dimensional model, Eq. (5) with spatially dependent Luttinger parameters²⁰⁻²² defined as follows. For the charge mode the Luttinger parameter is equal to K_{c+} inside the tube, $0 < x < L$, and unity in the leads. To zeroth order in $1/N$ the Luttinger parameters in the neutral modes are equal to unity both in the tube and in the leads.

We denote the THz electric field by $E_\omega(x)$. Its distribution along the wire depends on the details of the device geometry and is a solution of the proper electrodynamics problem which is beyond the scope of this paper; here we assume $E_\omega(x)$ is known. The dissipation rate of the electric field energy in the device can be written as

$$W(\omega) = \frac{1}{2} \text{Re} \int_0^L dx_1 \int_0^L dx_2 E_\omega(x_1) E_\omega^*(x_2) \sigma_\omega(x_1, x_2), \quad (6)$$

where $\sigma_\omega(x, x')$ is the nonlocal conductivity, which can be expressed via the retarded current-current correlation

function by the usual Kubo formula,

$$\sigma_\omega(x, x') = \frac{e^2}{\omega} \int_0^\infty dt e^{i\omega t} \langle [j(x, t), j(x', 0)] \rangle. \quad (7)$$

We assume that the electric field (i) varies smoothly on the scale of the lattice constant within the tube and (ii) preserves the reflection symmetry of the tube. Because of (i) it will not scatter electrons between the valleys, which involves momentum transfer $\sim 2Q$. Due to (ii) parity conservation also forbids backscattering of electrons within the same valley. Thus the electric field couples only to the smooth part of the current density, which can be expressed in the bosonized form as $j = 2\frac{e}{\pi} \partial_t \Phi_{c+}$. Therefore we can express the conductivity in terms of the Green's function of the Φ_{c+} field,

$$\sigma_\omega(x, x') = 4e^2 \frac{i\omega}{\pi^2} G_\omega^R(x, x'), \quad (8)$$

where

$$G_\omega^R(x, x') = -i \int_0^\infty dt e^{i\omega t} \langle [\Phi_{c+}(x, t), \Phi_{c+}(x', 0)] \rangle \quad (9)$$

is the retarded GF of the plasmon mode.

We denote the Green's function of the plasmon mode in the absence of backscattering by $G_{0,\omega}^R(x, x')$. It satisfies the differential equation

$$\left\{ \partial_x \left(\frac{v_F}{K^2(x)} \partial_x \right) + \frac{\omega^2}{v_F} \right\} G_{0,\omega}^R(x, x') = \pi \delta(x - x'), \quad (10)$$

with the boundary conditions: (1) $G_{0,\omega}^R(x, x')$ is continuous at $x = 0, L$ and $x = x'$; (2) $[v_F/K^2(x)] \partial_x G_{0,\omega}^R(x, x')$ is continuous at $x = 0, L$. For our model ($K(x)$ equal to K_{c+} inside the tube and unity outside) the Green's function can be expressed in terms of the reflection amplitude, $r = \frac{1-K_{c+}}{1+K_{c+}}$, of the plasmon from the junction with the lead.

The dissipated power in Eq. (6) depends only on the Green's function inside the tube. In this region for $0 < x < x' < L$ it is given by

$$G_{0,\omega}^R(x, x') = \frac{\pi K_{c+}}{2i\omega} \frac{e^{i\omega L/u}}{1 - r^2 e^{2i\omega L/u}} \left(e^{-i\frac{\omega}{u}x} + r e^{i\frac{\omega}{u}x} \right) \times \left(e^{i\frac{\omega}{u}(x'-L)} + r e^{-i\frac{\omega}{u}(x'-L)} \right). \quad (11)$$

In the region $0 < x' < x < L$ the Green's function is obtained by exchanging x and x' in the right hand side.

The Green's function above has poles as a function of frequency ω . The real part of the pole location gives the resonance frequency $\omega_n = n\pi u/L$, and its imaginary part gives the resonance half-width, γ_Z . The plasmon reflection amplitude from the junctions with the leads is determined by the ratio of the plasmon velocities in the tube and in the lead, $r = \frac{1-K_{c+}}{1+K_{c+}}$. This gives the escape half-rate $\gamma_Z = \frac{u}{L} \log \left(\frac{1+K_{c+}}{1-K_{c+}} \right)$. In the limit of high charge

stiffness, $K_{c+} \ll 1$, it becomes much smaller than the spacing between consecutive resonances and independent of the interaction strength, $\gamma_z \simeq 2K_{c+} \frac{u}{L} = 2v_F/L$.

The dissipated power is given by Eqs. (6), (8), and (11) and depends not only on the properties of the tube but also on the spatial distribution of the electric field (as mentioned above, the latter depends on the geometry and is assumed known).

IV. PLASMON DECAY IN THE DEVICE

The energy dissipation described by the ac conductance obtained in Sec. III corresponds to the emission of plasmon waves into the leads. The THz electric field excites plasmon modes of the electron fluid, which after a few reflections from the contacts with the leads are radiated out into the leads. Thus the energy absorbed from the THz radiation is re-radiated into the leads in the form of a plasmon flux.

In the presence of backscattering interactions, there is an additional contribution to the dissipation energy in the device. The plasmon waves generated by the THz radiation can decay into neutral modes before escaping into the leads. In this dissipation channel the absorbed energy is carried into the leads by the neutral modes. We discuss the microscopic interactions responsible for the decay of plasmons into the neutral modes in Sec. IV A and study how these processes modify the device conductance in Sec. IV B.

A. backscattering processes leading to plasmon decay

The possible backscattering processes obey certain symmetry selection rules. In particular parity conservation forbids single electron backscattering in armchair carbon nanotube due to e-e Coulomb interaction, which also attributes to the Klein paradox in graphene¹⁹ but two, or more generally, any even number of particles can be back-scattered. The electron interaction Hamiltonian contains such processes but their dimensionless coupling constants are small in $1/N$ and can be treated perturbatively. Having in mind temperatures well below the gap between the one-dimensional subbands ($v_F/R \sim 1\text{eV}$) we retain only the most relevant backscattering interactions. Namely the processes, which scatter two right movers into two left movers or vice-versa^{14,15,23}. Although for the Brillouin zone shown in Fig. 3 b) such scattering conserves quasimomentum and thus corresponds to normal processes, we refer to it as Umklapp scattering, following the accepted nanotube terminology^{14,15,23}.

In the bosonized representation the Umklapp Hamil-

tonian density can be written as²⁴

$$\begin{aligned} \mathcal{H}_u = & - \frac{\cos(2\Phi_{c+} - 4k_F x)}{2(\pi\xi)^2} \{g_3 \cos(2\Theta_{s-}) + \\ & (g_3 - g_1) \cos(2\Phi_{s+}) + \\ & g_1 [\cos(2\Phi_{c-}) - \cos(2\Phi_{s-})]\}. \end{aligned} \quad (12)$$

where the coupling constants originate from the short range part of the Coulomb interaction. They can be expressed in terms of the matrix elements of Coulomb interaction between electrons residing in the A and B sublattices, $V_{AA}(q)$ and $V_{AB}(q)$, as follows: $g_3 = V_{AA}(2Q) + V_{AB}(2Q)$ and $g_1 = V_{AA}(0) - V_{AB}(0)$ ^{23,24}. Here $2Q$ is the momentum difference between the two Dirac points, see Fig. 3, and we assumed that the Fermi momentum due to finite doping is small, $k_F \ll Q$. Both g_1 and g_3 arise from distances on the order of the lattice constant and are on the order of e^2/N .

In the presence of phonons single electron backscattering can occur because of electron-phonon interaction. The phonon modes in carbon nanotubes are classified to two types by the parity symmetry: *i*) transverse acoustic (TA), longitudinal optical (LO), and radial optical (RO) with negative parity, and *ii*) transverse optical (TO), longitudinal acoustic (LA), and radial acoustic (RA) with positive parity^{25,26,28}. The couplings of radial phonon modes to electrons are weaker in $1/N$ ^{26,28} than those for other phonon modes. Therefore we neglect their effects here. For the remaining couplings, one can distinguish between inter-valley and intra-valley scattering. The former requires a phonon with a momentum on the order of the inverse lattice spacing. Such phonons have high frequencies $\sim 10^3 K$ and are frozen out at room temperature. We thus neglect such processes and consider only intra-valley backscattering. Such processes change the parity of the electron wavefunction and thus require phonons with negative parity, i.e., TA or LO phonons. Their displacements are illustrated in Fig. 3. Since the frequency of the LO phonon is $\sim 1000 K$ it is frozen out in the temperature range we are interested in. Thus below we restrict our treatment to the backscattering of electrons from the TA phonons only.

The Hamiltonian of the TA phonon mode is given by

$$H_{TA} = \frac{1}{2} \int dx \left[\frac{1}{s_T} (\dot{\varphi}_T(x))^2 + s_T (\partial_x \varphi_T(x))^2 \right]. \quad (13)$$

Here $\varphi_T(x) = \sqrt{\rho s_T} u_T(x)$ is the dimensionless TA phonon field, ρ the linear mass density along the tube axis, $u_T(x)$ - the atomic displacement of the TA phonon mode, and $s_T \sim 1.4 \times 10^4$ m/s is the phonon velocity. The deformation of the TA mode couples to the time-reversal invariant operator bilinear in the fermions $M(x) = -i \sum_{\alpha r \sigma} \alpha r \psi_{\alpha r \sigma}^\dagger(x) \psi_{\alpha -r \sigma}$,

$$H_{ep} = \int dx M(x) g_T \partial_x \varphi_T(x). \quad (14)$$

In the bosonized representation the Hamiltonian density for the electron-TA phonon coupling can be written

as²⁸

$$\mathcal{H}_{ep} = -\frac{4g_T}{\pi\xi}\partial_x\varphi_T\left[\prod_{\nu=\pm}\cos(\Phi_{c+}-2k_Fx)\cos(\Phi_{c-})\sin(\Phi_{s\nu})\right. \\ \left.+\prod_{\nu=\pm}\sin(\Phi_{c+}-2k_Fx)\sin(\Phi_{c-})\cos(\Phi_{s\nu})\right], \quad (15)$$

where g_T is the e-ph coupling constant. Within the tight-binding model, the coupling constant g_T can be expressed in terms of the derivative of the transfer integral $J(r)$ with respect to the bond length r , see Ref. 25. In an armchair carbon nanotube, $g_T = \frac{\sqrt{3}}{4}\frac{a}{\sqrt{\rho s_T}}\frac{\partial J(r)}{\partial r}\Big|_0$ and for (N, N) armchair nanotubes, $\rho = 4NM/a$, where M is carbon atom mass and a is the lattice constant of a graphene sheet.

B. intrinsic energy dissipation in the device and plasmon decay

The backscattering interactions lead to the possibility of plasmon decay into the neutral modes. Using the fact that the backscattering interactions are small in $1/N$ we evaluate the decay rate and the corresponding correction to the device conductance using perturbation theory. We work in the regime where the cumulative plasmon decay rate in the device is smaller than the rate of elastic escape of plasmons into the leads. In this case the correction to the device conductance due to plasmon decay can be treated perturbatively.

Both the Umklapp and the electron-phonon backscattering interactions are expressed in terms of exponentials of the charge mode, Φ_{c+} . As a result, their contribution to the plasmon decay and the device conductance can be evaluated along similar lines.

To second order in perturbation theory there is no cross-correlation between the Umklapp and electron phonon backscattering processes, and the retarded Green's function of the charge mode can be expressed as

$$G_\omega^R(x, x') = G_{0,\omega}^R(x, x') + \sum_\eta \int_0^L dx_1 \int_0^L dx_2 G_{0,\omega}^R(x, x_1) \times \\ \mathcal{K}_\eta^\omega(x_1, x_2) G_{0,\omega}^R(x_2, x'), \quad (16)$$

where the index η denotes either the Umklapp ($\eta = u$) or the electron-phonon ($\eta = ep$) interaction, and the kernel $\mathcal{K}_\eta^\omega(x_1, x_2)$ can be expressed in terms of the retarded correlation function of the corresponding backscattering perturbation as

$$\mathcal{K}_\eta^\omega(x, x') = -ia_\eta^2 \int dt [e^{i\omega t} \langle [\mathcal{H}_\eta(x, t), \mathcal{H}_\eta(x', 0)] \rangle_0 - \int_0^L d\xi \langle [\mathcal{H}_\eta(x, t), \mathcal{H}_\eta(\xi, 0)] \rangle_0 \delta(x - x')] \quad (17)$$

Here a_η is the coefficient in the exponential dependence, $\sim (e^{ia_\eta\Phi_{c+}} + h.c.)$, of the corresponding backscattering perturbation on the charge field Φ_{c+} . The derivation of Eqs. (16) and (17) is outlined in Appendix A. The first term in Eq. (16) is the Green's function of the plasmon in the Luttinger liquid approximation, Eq. (11). The remaining terms represent correction due to backscattering interactions. The first term in the right hand side of Eq. (17) corresponds to the usual RPA-like diagram, the second term comes from the tadpole diagram and describes elastic scattering. The average $\langle \dots \rangle_0$ is performed with respect to the quadratic Luttinger liquid Hamiltonian, Eq. (5).

In the spatially inhomogeneous setup considered here the kernel $\mathcal{K}_\eta^\omega(x_1, x_2)$ depends not only on the coordinate difference but also on the center of mass coordinate $(x_1 + x_2)/2$. Its evaluation leads to rather cumbersome expressions. The situation simplifies in the physically relevant regime, where the characteristic thermal wavelength of the neutral modes, $L_T = v_F/T$, is much shorter than the size of the device L , while the wavelength of the plasmon resonance is on the order L .

In this case the Green's functions of the plasmon mode in the second term of Eq. (16) depend on x_1 and x_2 on the scale of wavelength of the plasmon resonance, $\sim L$. On the other hand, because backscattering operators depend exponentially on the neutral modes, $H_\eta(x, t) \sim \exp(ia_\eta\Phi_j(x, t))$, their correlator $\mathcal{K}_\eta^\omega(x_1, x_2)$ falls off exponentially for $|x_1 - x_2| > L_T$, which is much shorter than the length of the tube L . This is especially apparent in the case of a uniform wire for which the correlators of exponentials of bosonic fields have a simple form¹⁷,

$$\left\langle e^{ia\Phi_j(x,t)} e^{-ia\Phi_j(0,0)} \right\rangle_0 \equiv \Pi(K_j, a; x, t) = \frac{(\pi\xi TK_j/v_F)^{a^2 K_j/2}}{\{\sinh[\pi T(K_j x/v_F - t_-)] \sinh[\pi T(K_j x/v_F + t_-)]\}^{a^2 K_j/4}}, \quad (18)$$

where $t_- = t - i\epsilon$.

In the inhomogeneous situation the kernel $\mathcal{K}_\eta^\omega(x_1, x_2)$

still decays exponentially for $|x_1 - x_2| > L_T$. Therefore the main contribution to the Green's function correction

in Eq. (16) comes from the region $|x_1 - x_2| \lesssim L_T$. At such separations only the fluctuations of bosonic modes with wavelengths less than L_T contribute to the correlator. In the regime of interest, $L_T \ll L$, such short wavelength vibrations can be described semiclassically and are insensitive to the boundary conditions at the junctions, which describe reflection processes³⁴. Thus we come to the conclusion that in the bulk of the nanotube, i.e. with the exception of the regions of size L_T near the junctions the correlator $\mathcal{K}_\eta^\omega(x_1, x_2)$ is the same as in a homogeneous tube, and can be replaced by the local kernel

$$\mathcal{K}_\eta^\omega(x_1, x_2) \rightarrow \delta(x_1 - x_2) \mathcal{K}_\eta^\omega(q = 0), \quad (19)$$

where

$$\begin{aligned} \mathcal{K}_\eta^\omega(q = 0) &= -ia_\eta^2 \int_{-\infty}^{\infty} dx \int_0^{\infty} dt (e^{i\omega t} - 1) \\ &\times \langle [\mathcal{H}_\eta(x, t), \mathcal{H}_\eta(0, 0)] \rangle_0. \end{aligned} \quad (20)$$

This observation enables us to express the correction to the dissipated power due to decay of plasmons into neutral modes in terms of intrinsic parameters of uniform nanotubes. Accordingly, below all correlation functions of backscattering operators will be evaluated for infinite homogeneous nanotubes.

With the aid of Eq. (19) the power dissipation rate in Eq. (6) can be written in the form

$$W(\omega) = W_0(\omega) + \text{Im} \sum_{\eta} \mathcal{K}_\eta^\omega(q = 0) F(\omega). \quad (21)$$

Here the first term corresponds to the dissipation rate due to the escape of plasmon to the leads and is given by

$$\begin{aligned} W_0(\omega) &= \frac{2e^2\omega}{\pi^2} \int_0^L dx_1 \int_0^L dx_2 \\ &\times \text{Im} E_\omega(x_1) E_\omega^*(x_2) G_{0,\omega}^R(x_1, x_2). \end{aligned} \quad (22)$$

The second term in Eq. (21) corresponds to the intrinsic dissipation due to the electronic Umklapp processes and electron-phonon backscattering. It can be expressed in terms of kernel for an infinite tube, Eq. (20), and the form-factor $F(\omega)$,

$$\begin{aligned} F(\omega) &= \frac{2e^2\omega}{\pi^2} \int_0^L dx_1 \int_0^L dx_2 \int_0^L dx_3 E_\omega(x_1) E_\omega^*(x_3) \\ &\times G_{0,\omega}^R(x_1, x_2) G_{0,\omega}^R(x_2, x_3), \end{aligned} \quad (23)$$

which is quadratic in the THz electric field and depends, through its spatial distribution, on the geometry of the device.

Both the electric field and the unperturbed Green's function $G_{0,\omega}^R$ of the Luttinger liquid are temperature independent. Therefore $W_0(\omega)$ and the form-factor $F(\omega)$ do not depend on temperature. All the temperature dependence of the dissipation rate $W(\omega)$ is thus totally determined by intrinsic properties of a uniform CNT and is described by the kernel $\mathcal{K}_\eta^\omega(q = 0)$.

We note that the kernel $\mathcal{K}_\eta^\omega(q = 0)$ also determines the ac-conductivity $\sigma_\omega(q = 0)$ of an infinite wire¹⁷ in the high frequency or high temperature regime, where back-scattering interactions can be treated perturbatively. The latter can be expressed in the form

$$\sigma(\omega, T) = \frac{4e^2 K_{c+} u}{\pi(-i\omega + \sum_{\eta} \gamma_{\eta})}. \quad (24)$$

Here γ_{η} is the relaxation rate due to the Umklapp ($\eta = u$) or electron-phonon ($\eta = ep$) back-scattering, which can be expressed in terms of the local kernel as

$$\gamma_{\eta} \equiv \frac{i}{\omega} K_{c+} u_{c+} \mathcal{K}_\eta^\omega(q = 0). \quad (25)$$

Thus with the aid of Eqs. (21), (23) and (25) the temperature dependent part of the power dissipation in the device can be expressed in terms of the intrinsic plasmon decay rate in a uniform CNT, γ_{η} , which is given by Eqs. (25) and (20).

In the remainder of this section we evaluate the intrinsic plasmon decay rate due to various backscattering processes.

1. Umklapp mechanism of attenuation

We begin by considering Umklapp-mediated plasmon decay rate, γ_u . The Umklapp Hamiltonian density in Eq. (12) contains exponential operators of both Φ - and Θ -fields corresponding to the neutral modes. Because the Luttinger parameter K for neutral modes is equal to unity, the correlators of exponential operators of Φ - and Θ -fields coincide. As a result we obtain

$$\begin{aligned} \langle \mathcal{H}_u(x, t) \mathcal{H}_u(0, 0) \rangle_0 &= \frac{3g_1^2 + 2g_3^2 - 2g_1g_3}{16(\pi\xi)^4} \cos(4k_F x) \times \\ &\Pi(K_{c+}, 2; x, t) \Pi(1, 2; x, t). \end{aligned} \quad (26)$$

The analogous correlator corresponding to the opposite ordering of backscattering operators can be obtained from the identity

$$\langle \mathcal{H}_u(0, 0) \mathcal{H}_u(x, t) \rangle_0 = \langle \mathcal{H}_u(x, t) \mathcal{H}_u(0, 0) \rangle_0^*.$$

Using Eqs. (25), (20), (18), and (26) we obtain

$$\gamma_u = \left(\frac{\pi T \xi}{u} \right)^{2K_{c+}} \frac{3g_1^2 + 2g_3^2 - 2g_1g_3}{4T(\pi\xi)^2} F_u \left(\frac{\omega}{T}, \frac{v_F k_F}{T} \right), \quad (27)$$

where $F_u(\frac{\omega}{T}, \frac{v_F k_F}{T})$ is a scaling function depending on the ratio ω/T and $v_F k_F/T$. It is given by the following double integral,

$$F_u\left(\frac{\omega}{T}, \frac{v_F k_F}{T}\right) = \frac{T}{\omega} \int_{-\infty}^{\infty} dX \int_0^{\infty} dY \left(e^{i\frac{\omega}{T}Y} - 1\right) \cos\left(\frac{4k_F v_F}{T}X\right) \left[\frac{1}{(\sinh \pi(\frac{v_F}{u}X + Y_-) \sinh \pi(\frac{v_F}{u}X - Y_-))^{K_{c+}}} \frac{1}{\sinh \pi(X + Y_-) \sinh \pi(X - Y_-)} - c.c. \right], \quad (28)$$

where $Y_- \equiv Y - i\epsilon$.

Using the standard deformation of the integration contour, $Y_- \rightarrow Y - i/2$, in the above equation one may ex-

press the real part of the scaling function in the form that is more convenient for numerical evaluation,

$$\Re F_u\left(\frac{\omega}{T}, \frac{v_F k_F}{T}\right) = \frac{T}{\pi^2 \omega} \sinh \frac{\omega}{2T} \int_{-\infty}^{\infty} dx \int_{-\infty}^{\infty} dy \frac{\cos(y\omega/\pi T) \cos(4k_F v_F x/\pi T)}{[\cosh(K_{c+}x + y) \cosh(K_{c+}x - y)]^{K_{c+}} \cosh(x + y) \cosh(x - y)}. \quad (29)$$

In the limit of high charge stiffness, $K_{c+} \rightarrow 0$, the above expression simplifies to,

$$\Re F_u\left(\frac{\omega}{T}, \frac{v_F k_F}{T}\right) = \frac{\frac{T}{2\omega} \sinh \frac{\omega}{2T}}{\cosh\left(\frac{4k_F v_F}{4T}\right) \cosh\left(\frac{4k_F v_F - \omega}{4T}\right)}. \quad (30)$$

In the temperature regime of interest, $T \gg \omega \sim u/L$, the function $F_u(\frac{\omega}{T}, \frac{v_F k_F}{T})$ in Eq. (28) reaches the dc limit $F_u(0, \frac{v_F k_F}{T})$, which is purely real and depends only on the doping level. For comparison, in Fig. 4 we plot the static limit of the scaling function $F_u(0, k_F v_F/T)$ evaluated numerically at $K_{c+} = 0.2$ using Eq. (29) and the analytical expression from Eq. (30) for $K_{c+} = 0$.

At small doping, the scaling function goes to a constant and γ_u exhibits a power law dependence on the temperature, $\gamma_u \sim T^{2K_{c+}-1}$. At strong doping, $2k_F v_F > T$ the scaling function acquires an activated temperature dependence. This results in exponential decay of $\gamma_u \sim T^{2K_{c+}-1} \exp(-2k_F v_F/T)$. The physical reason for the exponential temperature decay can be understood from simple inspection of energy and momentum conservation, which shows that energetically optimal process involves backscattering of two thermal quasiparticles exactly at the Dirac point $k = Q$. At strong doping, $k_F v_F \gg T$ the occupancy of such states is exponentially small, $\sim \exp(-2k_F v_F/T)$.

Equation (27) and the subsequent equations express the plasmon decay rate γ_u in terms of the somewhat arbitrary short distance cutoff, ξ , which has the order of the radius of carbon nanotube. Alternatively, γ_u can be expressed in a renormalized form as a function of an intrinsic cutoff-independent low energy scale. In the case of Umklapp interactions the role of such a low energy scale is played by the Umklapp gap. Namely, the Umklapp interaction is a relevant perturbation relative to the Luttinger liquid fixed point and drives the system to a

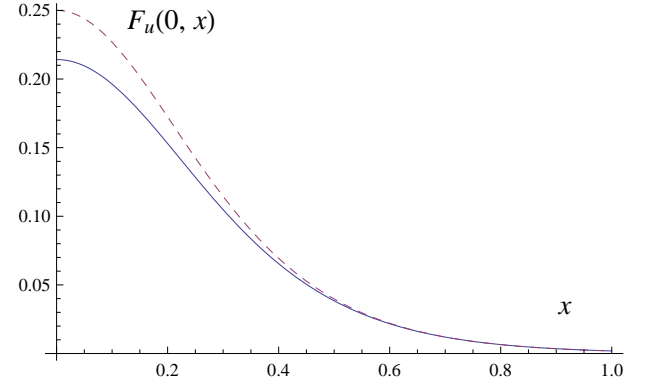


FIG. 4: Dependence of the scaling function in the static limit, $F_u(0, x)$ on the doping parameter $x = \frac{k_F v_F}{T}$ for $K_{c+} = 0.2$ (solid line) and $K_{c+} = 0$ (dashed line).

Mott insulating state with the gap²³,

$$\Delta_u \sim \frac{v_F}{\xi} \left(\frac{g_u}{v_F}\right)^{1/(1-K_{c+})}.$$

Here $g_u \sim e^2/N$ is the strength of the Umklapp interaction. This gap depends on the radius of the CNT as $R^{-[1+1/(1-K_{c+})]}$ and is hard to evaluate theoretically due to the ambiguity of the coupling constant, but numerical results estimate that it's of the order of 1 – 10 meV for an armchair CNT of radius ~ 1 nm²³. For the perturbation calculation to be applicable, the temperature we consider should be above the Umklapp gap. Up to a numerical coefficient on the order unity the plasmon decay rate in Eq. (27) can be expressed in terms of this gap as

$$\gamma_u \sim \Delta_u \left(\frac{T}{\Delta_u}\right)^{2K_{c+}-1} F_u\left(\frac{\omega}{T}, \frac{v_F k_F}{T}\right). \quad (31)$$

At zero doping, $\gamma_u \sim T$ for $K_{c+} \rightarrow 1$, i.e., without

considering the Luttinger liquid effect. Yet in the Luttinger liquid description with strong Coulomb interaction, $K_{c+} \rightarrow 0$, $\gamma_u \sim \Delta_u^2/T$.

Note that according to Eqs. (24) and (31) the Umklapp processes yield $\sigma(\omega = 0, T) \propto T^{1-2K_{c+}}$ at zero doping and high temperature, which is consistent with the result obtained in a previous work¹⁴. In the case $K_{c+} \rightarrow 1$, i.e., in the absence of Luttinger liquid effects, the decay rate due to Umklapp processes $\gamma_u \sim T$, and the resistivity has linear dependence on temperature at high temperature, which is consistent with the perturbative calculation of plasmon decay rate from Umklapp processes in CNTs^{13,27}. We can see that the inclusion of the long range interaction significantly modifies the dependence of the plasmon decay rate on temperature due to Umklapp processes. In the case of strong Coulomb interaction, i.e., $K_{c+} \rightarrow 0$, the temperature dependence of decay rate is strongly modified and becomes $\gamma_u \sim T^{-1}$ at high temperature.

2. Phonon-assisted mechanism of attenuation

We now consider plasmon decay rate due to electron-phonon interactions, γ_{ep} . Its physical mechanism can be understood as follows. Parity-breaking deformations in the TA mode cause single particle backscattering, which causes the plasmon decay. Due to the presence of the adiabatic parameter $s_T/v_F \sim 2 \times 10^{-2} \ll 1$ the lattice deformations are effectively static. Thus the energy of the decaying plasmon is transferred into the neutral modes of the electron liquid. Therefore this mechanism, which we analyze below, may be characterized as phonon-assisted plasmon decay. In two dimensions it has been studied in Ref. 33. At finite doping single electron backscattering involves phonons with momentum $2k_F$. With the exception of very low temperatures, $T < 2k_F s_T$, the occupation numbers of such phonons are large, $\sim T/2k_F s_T$. This corresponds to classical thermal fluctuations of the lattice. Since the probability of such fluctuations is determined by the elastic energy $\sim \exp(-s_T \int dx [\partial_x \phi_T(x)]^2/2T)$, the one-electron backscattering potential $\sim \partial_x \phi_{TA}(x)$ (see Eq. (14)) may be viewed as δ -correlated in space. More precisely, the correlator of backscattering potential $\sim \partial_x \phi_{TA}(x)$ becomes exponentially small at distances greater than s_T/T , as is clear from Eq. (33) below. As the electron correlators depend on the spatial coordinates on much larger scales $\sim L_T \gg s_T/T$ the correlator of deformation

potentials becomes effectively short range. In this respect the phonon-assisted plasmon decay mechanism is similar to that induced by a short range disorder potential. The temperature dependence of disorder-induced conductivity was obtained in Ref. 16, $\sigma_{dis} \sim \langle V^2 \rangle T^{(K_{c+}-1)/2}$, where $\langle V^2 \rangle$ is the variance of the random potential. In contrast to the temperature-independent variance of the disorder potential, the variance of the phonon correlator scales linearly with the temperature. This gives the power law $\gamma_{ep} \sim T^{(1+K_{c+})/2}$, which is confirmed by the calculations below.

The phonon-assisted decay rate γ_{ep} can be evaluated similarly to the case of Umklapp processes. Using Eq. (18) we obtain the following expression for the correlation function for the electron-phonon Hamiltonian densities given by Eq. (15),

$$\begin{aligned} \langle \mathcal{H}_{ep}(x, t) \mathcal{H}_{ep}(0, 0) \rangle &= 2 \left(\frac{g_T}{\pi \xi} \right)^2 \cos(2k_F x) D_{ph}(x, t) \\ &\times \prod_j \Pi(K_j, 1; x, t), \end{aligned} \quad (32)$$

where $j = c\pm, s\pm$, and $D_{ph}(x, t) \equiv \langle \nabla \varphi_T(x, t) \nabla \varphi_T(0, 0) \rangle$ is the phonon correlator given by

$$D_{ph}(x, t) = - \sum_{\nu=\pm 1} \frac{(\pi T/s_T)^2}{2 \sinh^2[\pi T(\frac{x}{s_T} + \nu t_-)]}. \quad (33)$$

The correlator with opposite ordering can be obtained from Eq. (32) using the identity $\langle \mathcal{H}_{ep}(0, 0) \mathcal{H}_{ep}(x, t) \rangle = \langle \mathcal{H}_{ep}(x, t) \mathcal{H}_{ep}(0, 0) \rangle^*$.

Substituting Eqs. (32), (18) and (33) into Eq. (20) and using Eq. (25) we obtain the phonon-assisted rate γ_{ep} . While carrying out the spatial integration in Eq. (20) we may neglect the position dependence in the electronic correlation functions and replace them by $\Pi(K_j, 1; x = 0, t)$ (this is justified by the small value of the adiabatic parameter s_T/v_F). Doing so we obtain

$$\gamma_{ep} = \tilde{g}_T^2 \frac{\pi v_F}{\xi} \left(\frac{\pi T \xi}{v_F} \right)^{\frac{1}{2}} \left(\frac{\pi T \xi}{u} \right)^{\frac{K_{c+}}{2}} F_{ep} \left(\frac{\omega}{T}, \frac{s_T k_F}{T} \right), \quad (34)$$

where $\tilde{g}_T \equiv g_T/\sqrt{s_T v_F}$ is the dimensionless coupling constant of e-ph interaction, $F_{ep}(\frac{\omega}{T}, \frac{s_T k_F}{T})$ is the scaling function for the phonon-assisted decay rate. Introducing dimensionless variables $X = xT/s_T$ and $Y = Tt$ we can express it as

$$\begin{aligned} F_{ep} \left(\frac{\omega}{T}, \frac{s_T k_F}{T} \right) &= \frac{T}{\omega} \int_0^\infty dY \int_{-\infty}^\infty dX (e^{i\frac{\omega}{T}Y} - 1) \cos \left(\frac{2k_F s_T}{T} X \right) \\ &\left\{ \left[\frac{1}{\sinh^2(\pi(X+Y_-))} + \frac{1}{\sinh^2(\pi(X-Y_-))} \right] \left(\frac{1}{\sinh(\pi Y_-) \sinh(-\pi Y_-)} \right)^{\frac{3+K_{c+}}{4}} - c.c. \right\}. \end{aligned} \quad (35)$$

Similarly to the Umklapp case, the real part of the above scaling function can be expressed in a more convenient form,

$$\Re F_{ep} \left(\frac{\omega}{T}, \frac{s_T k_F}{T} \right) = \frac{T}{\pi^2 \omega} \sinh \frac{\omega}{2T} \int_{-\infty}^{\infty} dy \int_{-\infty}^{\infty} dx \left[\frac{1}{\cosh^2(x+y)} + \frac{1}{\cosh^2(x-y)} \right] \frac{\cos \frac{\omega y}{\pi T} \cos \frac{2k_F s_T x}{\pi T}}{(\cosh y)^{(3+K_{c+})/2}}. \quad (36)$$

From the above equations it is clear that the phonon-assisted decay rate is practically unaffected by doping as long as $T > 2k_F s_T$. Because of the slow velocity s_T of the phonon mode, with the exception of very low temperatures, this condition is satisfied for all practically accessible doping levels. In this regime Eq. (36) simplifies to

$$\Re F_{ep} \left(\frac{\omega}{T}, 0 \right) = \frac{2T}{\pi^2 \omega} \sinh \frac{\omega}{2T} 2^{\frac{3+K_{c+}}{2}} \times B \left(\frac{3+K_{c+}}{4}, \frac{i\omega}{2\pi T}, \frac{3+K_{c+}}{4} + \frac{i\omega}{2\pi T} \right). \quad (37)$$

In the limit $\omega \ll T$, the scaling function goes to a constant, $F_{ep}(0, 0) = 2^{\frac{3+K_{c+}}{2}} B([3+K_{c+}]/4, [3+K_{c+}]/4)/\pi^2$.

Similarly to the case of Umklapp processes the phonon assisted decay rate can be expressed in terms a renormalized form, which does not involve the short distance cutoff. In this case the role of the low energy scale for the electron-phonon interaction with the TA mode is played by the twist Peierls gap²⁸, $\Delta_{ep} \sim \frac{v_F}{\xi} \tilde{g}_T^{4/(1-K_{c+})}$, which depends on the radius of the CNT as $\sim R^{-(1+2/(1-K_{c+}))}$ and in the limiting case $K_{c+} \rightarrow 0$ is on the order of a few tens of Kelvin for a (5, 5) armchair CNT. This gap is induced by the Peierls instability of the armchair tube with respect to a twist distortion²⁸⁻³⁰. Up to a numerical coefficient on the order unity the phonon-assisted decay rate can be expressed in terms of the twist Peierls gap as,

$$\gamma_{ep} \sim \Delta_{ep} \left(\frac{T}{\Delta_{ep}} \right)^{\frac{1+K_{c+}}{2}} F_{ep} \left(\frac{\omega}{T}, \frac{s_T k_F}{T} \right). \quad (38)$$

In the dc limit and at zero doping, the Luttinger liquid effects manifest themselves by changing the power dependence of γ_{ep} or resistivity from $\gamma_{ep} \sim T$ for non-interacting case³¹ to $\gamma_{ep} \sim T^{\frac{1+K_{c+}}{2}}$ in a Luttinger liquid at temperatures above the Peierls gap. Experiments on phonon-induced resistivity to date^{31,32} have been conducted on CNTs placed on substrates rather than freely suspended CNTs, and exhibit linear temperature dependence of resistivity, consistent with the non-interacting electron approximation, $K_{c+} = 1$.

V. SUMMARY OF THE RESULTS

We studied the intrinsic plasmon decay rates in clean armchair nanotubes. Plasmon oscillations decay into

neutral electron modes. Such processes are facilitated by electron-electron and electron-phonon backscattering processes. In second order of perturbation theory in the backscattering interactions the total decay rate is given by the sum of partial decay rates due to each mechanism. For undoped CNT, both electron-electron and electron-phonon rates reveal power law dependence on the frequency of oscillations or the temperature of the system with non-integer exponent, that depends on the Luttinger liquid parameter K_{c+} .

The plasmon decay processes lead to temperature dependent corrections to power dissipation in the device depicted in Fig. 2. Therefore they can be studied experimentally in a finite device by measuring the temperature dependence of power dissipation. In the regime where the temperature length $L_T = v_F/T$ is shorter than the plasmon wavelength the temperature-dependent part of the dissipated power can be expressed in terms of the intrinsic plasmon decay rate γ in homogeneous nanotube using Eqs. (21-23) and (25). Furthermore, in this regime γ can be related to the intrinsic ac conductivity of carbon nanotubes via Eq. (24). Thus intrinsic plasmon decay rate in CNT can, in principle, be extracted from measurements in finite size devices.

Among the electron-electron interactions resulting in plasmon decay the most relevant ones are Umklapp processes. They correspond to backscattering of pairs of electrons and lead to the decay rate that scales as $\gamma_u \sim T^{2K_{c+}-1}$ at zero doping and becomes exponentially small, $\sim \exp(-2k_F v_F/T)$, at large doping, see Eq. (27). This rate can be expressed in terms of the short distance cutoff and Umklapp coupling constants, see Eq. (27) or in terms of the cutoff-independent Umklapp gap, as in Eq. (31).

In contrast to the Umklapp processes, the phonon-assisted decay rate depends on the doping level only on a very large scale $v_F k_F \sim T v_F / s_T \approx 0.6 \times 10^2 T$. With the exception of rather low temperatures the practically achievable doping levels lie below this scale. In this regime the phonon-assisted decay rate scales as $\gamma_{ep} \sim T^{(1+K_{c+})/2}$, as given by Eq. (34). It can also be expressed in terms of a cutoff-independent energy scale Δ_{ep} associated with electron-phonon interactions, see Eq. (38). This scale is given by the gap in the electron spectrum induced by the twist Peierls instability.

If the plasmon frequency is smaller than the temperature, the ratio of the phonon-assisted rate and the Umklapp one at zero doping is $\gamma_{ep}/\gamma_u \sim \left(\frac{T^3 \Delta_{ep}}{\Delta_u^4} \right)^{\frac{1-K_{c+}}{2}}$. The phonon assisted decay is dominant in the wide range of temperatures, $T > (\Delta_u^4 / \Delta_{ep})^{1/3}$. With the exception

of the region of very low temperatures it is dominated by electron-phonon scattering and scales as $T^{(1+K_{c+})/2}$. This is consistent with the temperature dependence of phonon-induced resistivity¹⁴.

We are grateful to David Cobden, Dan Prober and Xiaodong Xu for useful discussions. This work was supported by the DOE grants DE-FG02-07ER46452 (W.C. and A.V.A) and DE-FG02-06ER46313 (E.G.M.) NSF DMR Grant No. 0906498 at Yale University (L.I.G.), and the Nanosciences Foundation at Grenoble, France. The hospitality of CEA Grenoble (France) and the Institute for Nuclear Theory at the University of Washington

(Seattle) is greatly appreciated.

Appendix A: fusion rules

Equation (16) can be derived by noting that both the Umklapp and electron-phonon backscattering Hamiltonian densities have exponential dependence of the charge field Φ_{c+} , $\sim (e^{ia_\eta\Phi_{c+}} + h.c.)$ and using the following identity that holds for Gaussian averages,

$$\begin{aligned} & \langle \phi_{c+}(x) e^{ia_\eta\phi_{c+}(x_1)} e^{-ia_\eta\phi_{c+}(x_2)} \phi_{c+}(x') \rangle_0 = \\ & - (ia_\eta)^2 \langle \phi_{c+}(x) \phi_{c+}(x_1) \rangle_0 \langle e^{ia_\eta\phi_{c+}(x_1)} e^{-ia_\eta\phi_{c+}(x_2)} \rangle_0 \langle \phi_{c+}(x_2) \phi_{c+}(x') \rangle_0 \\ & + (ia_\eta)^2 \langle \phi_{c+}(x) \phi_{c+}(x_1) \rangle_0 \langle e^{ia_\eta\phi_{c+}(x_1)} e^{-ia_\eta\phi_{c+}(x_2)} \rangle_0 \langle \phi_{c+}(x_1) \phi_{c+}(x') \rangle_0 + \\ & \text{same terms with } x_1 \leftrightarrow x_2 + \langle \phi_{c+}(x) \phi_{c+}(x') \rangle_0 \langle e^{ia_\eta\phi_{c+}(x_1)} e^{-ia_\eta\phi_{c+}(x_2)} \rangle_0. \end{aligned} \quad (A1)$$

This formula can be established by expanding the exponentials in the left hand side in the Taylor series and applying Wick's theorem to each term. The resulting series sums to the expression in the right hand side.

The last term in the right hand side corresponds to a disconnected diagram and does not contribute to the correlation function.

-
- ¹ M. S. Purewal *et al*, Phys. Rev. Lett. **98**, 186808 (2007).
 - ² S. M. Bachilo *et al.*, Science **298**, 2361 (2002).
 - ³ J. Lefebvre, Y. Homma, and P. Finnie, Phys. Rev. Lett. **90**, 217401(2003)
 - ⁴ A. Hagen and T. Hertel, Nano Lett. **3**, 383 (2003).
 - ⁵ O. J. Korovyanko *et al*, Phys. Rev. Lett. **92**, 017403(2004)
 - ⁶ P. Avouris, M. Freitag, V. Perebeinos, Nature Photonics, **2**, 341(2008).
 - ⁷ C. Kramberger, *et al.*, Phys. Rev. Lett. **100**, 196803 (2008).
 - ⁸ Z. Zhong, N. M. Gabor, J. E. Sharping, A. L. Gaeta, P. L. McEuen, Nature Nanotechnology, **3**, 201 (2008).
 - ⁹ M. Bockrath, D.H. Cobden, J.G. Lu, A. G. Rinzler, R.E. Smalley, L. Balents, and P.L. McEuen, Nature **397**, 598 (1999).
 - ¹⁰ Z. Yao, H. W. Ch. Postma, L. Balents, C. Dekker, Nature **402**, 273 (1999).
 - ¹¹ G. D. Mahan, *Many particle physics*, Kluwer Academic/Plenum Publishers (2000).
 - ¹² D. Prober, private communication
 - ¹³ L. Balents and M. P. A. Fisher, Phys. Rev. B **55**, R11973 (1997).
 - ¹⁴ C. Kane, L. Balents, and M. P. A. Fisher, Phys. Rev. Lett. **79**, 5086 (1997).
 - ¹⁵ R. Egger and A. Gogolin, Phys. Rev. Lett. **79**, 5082 (1997).
 - ¹⁶ H. Yoshioka Phys. Rev. B **61**, 7316 (2000).
 - ¹⁷ T. Giamachi, *Quantum physics in one dimension*, Clarendon Press (2003).
 - ¹⁸ A. M. Tsvelik, *Quantum Field Theory in Condensed Matter Physics*, Cambridge 2003.
 - ¹⁹ M. I. Katsnelson, K. S. Novoselov and A. K. Geim, Nature Physics, **2** 620 (2006).
 - ²⁰ D. L. Maslov and M. Stone, Phys. Rev. B **52**, 5539 (1995).
 - ²¹ V. V. Ponomarenko, Phys. Rev. B **52**, R8666 (1995).
 - ²² I. Safi and H. J. Schulz, Phys. Rev. B **52**, R17040 (1995).
 - ²³ A. Odintsov and H. Yoshioka, Phys. Rev. B **59**, 10457 (1999).
 - ²⁴ A. A. Nersesyan and A. M. Tsvelik, Phys. Rev. B **68**, 235419 (2003).
 - ²⁵ R. Jishi, M. S. Dresselhaus and G. Dresselhaus, Phys. Rev. B **48**, 11385 (1993).
 - ²⁶ G. Mahan, Phys. Rev. B **68**, 125409 (2003).
 - ²⁷ E. G. Mishchenko, L. I. Glazman, *unpublished*
 - ²⁸ W. Chen, A. V. Andreev, A. M. Tsvelik, and D. Orgad, Phys. Rev. Lett. **101**, 246802 (2008).
 - ²⁹ M.T. Figge, M. Mostovoy, and J. Knoester, Phys. Rev. Lett. **86**, 4572 (2001); Phys. Rev. B **65**, 125416 (2002).
 - ³⁰ H. Suzuura, and T. Ando, pp. 1625-1626, in *Proc. of 25th Internat. Conf. on Phys. of Semiconductors*. {Eds. N. Miura and T. Ando} (Springer, 2001).
 - ³¹ C. L. Kane *et al*, Europhys. Lett., **41**(6), 683 (1998).
 - ³² J. Y. Park *et al*, Nano Lett. **4**, 517 (2004).
 - ³³ E. G. Mishchenko, M. Yu. Reizer, and L. I. Glazman Phys. Rev. B **69**, 195302 (2004).
 - ³⁴ The quasiclassical treatment becomes inapplicable in the regions within L_T of one of the junctions, but the contribution of these regions to the overall decay rate is small as compared to that of the rest of the tube.